Vaasan yliopisto
UNIVERSITY OF VAASA
OSUVA Open Science

This is a self-archived – parallel published version of this article in the publication archive of the University of Vaasa. It might differ from the original.

Optimization of temperature parameters for the autothermic pyrolysis in-situ conversion process of oil shale

Author(s): Xu, Shaotao; Lü, Xiaoshu; Sun, Youhong; Guo, Wei; Li, Qiang; Liu, Lang; Kang, Shijie; Deng, Sunhua

Title: Optimization of temperature parameters for the autothermic pyrolysis in-situ conversion process of oil shale

Year: 2022

Version: Accepted Manuscript

Copyright ©2022 Elsevier. This manuscript version is made available under the Creative Commons Attribution–NonCommercial–NoDerivatives 4.0 International (CC BY–NC–ND 4.0) license, https://creativecommons.org/licenses/by-nc-nd/4.0/

Please cite the original version:

Xu, S., Lü, X., Sun, Y., Guo, W., Li, Q., Liu, L., Kang, S. & Deng, S. (2022). Optimization of temperature parameters for the autothermic pyrolysis in-situ conversion process of oil shale. *Energy* 264, 126309. https://doi.org/10.1016/j.energy.2022.126309

Optimization of temperature parameters for the autothermic pyrolysis in-situ conversion process of oil shale

Shaotao Xu[a,b,c], Xiaoshu Lü[a,e,f], Youhong Sun[a,b,c,d,*], Wei Guo[a,b,c], Qiang Li[a,b,c], Lang Liu[g], Shijie Kang[h], Sunhua Deng[a,b,c,*]

[a] College of Construction Engineering, Jilin University, Changchun 130021, China

[b] National-Local Joint Engineering Laboratory of In-situ Conversion, Drilling and Exploitation Technology for Oil Shale, Jilin University, Changchun 130021, China

[c] Key Lab of Ministry of Natural Resources for Drilling and Exploitation Technology in Complex Conditions, Jilin University, Changchun 130021, China

[d] China University of Geosciences, Beijing 100083, China

[e] Department of Electrical Engineering and Energy Technology, University of Vaasa, P. O. Box 700, FIN-65101, Vaasa, Finland

[f] Department of Civil and Structural Engineering, School of Engineering, Aalto University, PO Box 12100, FIN-02015 Espoo, Finland

[g] Xian Univ Sci & Technol, Energy Sch, Xi'an 710054, China

[h] Ganjiang Innovation Academy, Chinese Academy of Sciences, Ganzhou 341000, China

* Corresponding author.

E-mail addresses: syh@jlu.edu.cn, denghua13@163.com

Abstract

In this study, a temperature optimization strategy for the Huadian oil shale

autothermal pyrolysis in-situ conversion process (ATS) was first proposed by systematically investigating the reaction characteristics of various semi-cokes. As the pyrolysis temperature rised, the semi-coke's calorific value was found to undergo three different stages of increasing, decreasing, and flattening, peaking at around 330 °C. Additionally, the semi-cokes formed at different temperatures exhibited similar combustion characteristics, including combustion activation energy, combustion characteristic parameters, and product release characteristics. Due to the serious pore blockage caused by the substantial generation and the ignition coking of the bitumen, the reaction characteristics of semi-cokes were dramatically decreased at about 330 °C. Finally, the relationship between in-situ heat generation and demand at various stages of ATS process was discussed, and a reasonable strategy for the screening of temperature parameters was proposed. According to this strategy, the optimal control temperature for the preheating stage was determined at 350–370 °C and at T_{act} (defined in 4.3.2) for the retorting zone in the reaction stage. The results of this study provide a new perspective on the theoretical foundation of the ATS process and have crucial guiding implications for practical engineering applications.

Key words: oil shale; kinetic analysis; combustion characteristics; heat relationship; temperature optimization.

1. Introduction

Due to its huge reserves and widespread distribution, oil shale (OS) is garnering increased interest as a promising alternative resource in the face of energy shortages

[1,2,3,4]. Generally, the liquid shale oil and gaseous hydrocarbons can be extracted from the kerogen in OS by heating it to 300–550 °C [5,6,7]. Compared to retort OS aboveground, directly heating the underground OS formation in an in-situ retorting procedure is more promising nowadays, since it does not require mining and avoids environmental disadvantages [8,9]. So far, more than a dozen in-situ OS conversion technologies have been researched and proposed [10,11].

However, challenges exist in the high pyrolysis temperature of OS and the low permeability and thermal conductivity of the OS formation [12]. In recent years, methods and technologies utilizing oxygen to assist in-situ OS exploitation have attracted growing attention and are regarded as one of the most promising in-situ OS conversion technologies due to the high thermal efficiency, short production cycle, and low exploitation cost [13–19]. Accordingly, considerable strategies have been proposed and studied, such as the co-current combustion method [13], self-heating retorting [14,15], topochemical reaction method [16,17], and co-current oxidizing pyrolysis [18,19]. These studies have demonstrated that oxygen can significantly promote the pyrolysis of OS and reduce the heating costs by consuming partial organic matter and residual carbon by-products to heat itself [20,21]. Simultaneously, high oil yield, excellent oil quality, and rapid production can be achieved [22,23]. Consequently, the application of oxygen is expected to help the OS industry achieve an important breakthrough.

In order to fully utilize the role of oxygen in the in-situ conversion of OS, an

autothermic pyrolysis in-situ conversion process (ATS) has been recently proposed and successfully pilot tested in Fuyu, Jilin Province, China. As indicated in Fig. 1, the ATS process is mainly separated into three stages: preheating stage, initiation stage, and reaction stage. First, the OS formation near the heat injection well is preheated to the target temperature (T_0) in an inert atmosphere during the preheating stage. Then the OS formation is ignited by injecting ambient air or other oxygen-containing gas from the heat injection well in the initiation stage. As a result, the formation of organic matters, oil and gas products, residual carbon, and other by-products near the heat injection well will react violently with oxygen. A large amount of reaction heat will be released, thus heating the OS at the far end within retorting zone to a particular pyrolysis temperature (T_1) and promoting the cracking and the release of hydrocarbon products. In this process, by controlling the air injection time, air flow rate, and other parameters, oxygen consumption can be constrained mainly in the combustion zone to produce gases such as carbon monoxide and carbon dioxide. Furthermore, due to the OS's compactness and low permeability, oxygen cannot easily access the front retorting zone during reaction process. As a result, the gases entering the pyrolysis area are primarily inert gases, such as nitrogen and carbon dioxide, and the anaerobic retorting reaction takes place primarily in the retorting zone. Finally, constant injection of air or other oxygen-containing gas keeps the reaction continuing and moving forward until the reaction area is advanced to the production well, constituting the reaction stage. By implementing the ATS process, a substantial

amount of shale oil and gas products can be successfully extracted, which demonstrates the feasibility and practicality of the ATS process.

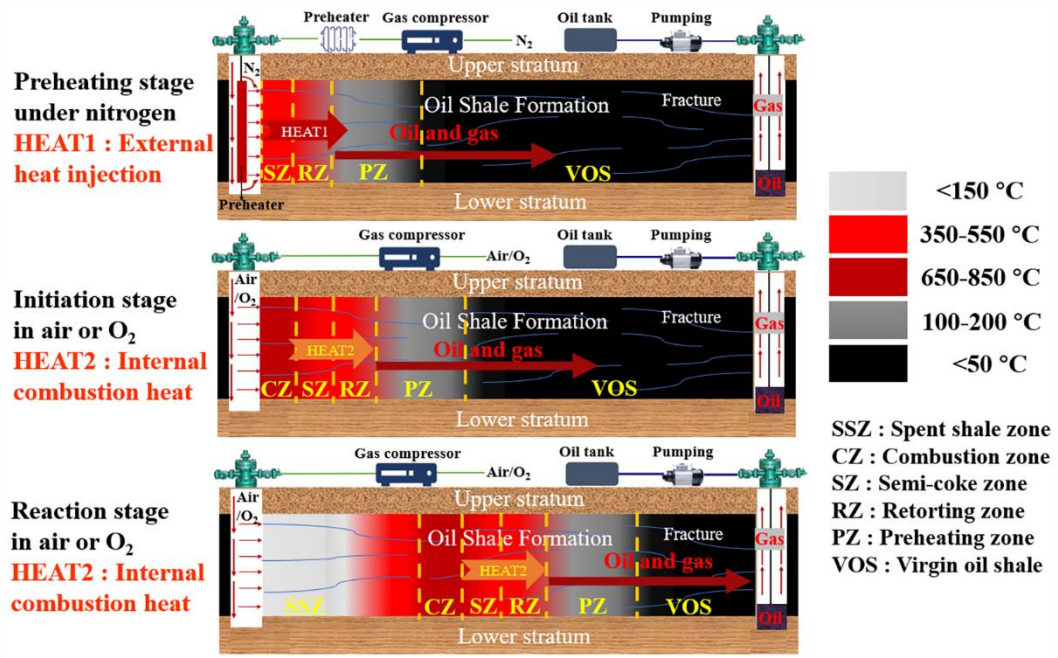

Fig. 1. Description of main stages during ATS process construction.

Notably, the success of ATS implementation relies on its ability to transition from the preheating stage to the initiation stage while maintaining a continuous self-heating reaction in the reaction stage. The oxidation exothermic reaction of the semi-coke product generated from the pyrolysis of OS is the main source of self-heating reaction. Hence, semi-coke combustion properties, such as calorific value, combustion activation energy, indices of combustion and product release, are critical for the successful switching and continuation of the underground reaction process. So far, many results on this issue have been published, including reaction atmosphere, combustion characteristics, kinetic analysis, and thermodynamic properties [24–34]. However, these studies have mostly concentrated on the semi-coke under the

pyrolysis temperatures of 400–1000 °C, which contains residual kerogen, residual carbon, heavy oil, and other by-products [20–24]. Due to the significant amount of internal volatile matter, the combustion of OS is considered homogeneous, while the combustion of semi-coke formed at high temperature will become heterogeneous [25,26]. TG/DTG techniques are frequently used to investigate the combustion kinetics and properties of semi-cokes [27,28]. The results show that the combustion performance of semi-coke decreases as the temperature rises at 400–1000 °C [29]. Moreover, OS's thermal decomposition and combustion process exhibits many reaction pathways, and the variety of organic and mineral components in OS has a significant impact on the thermal behavior and kinetic properties of different samples [30]. The heating temperature also affects semi-coke's chemical composition and pore evolution, and the elimination of volatile materials results in a rough and irregular pore surface [31,32]. At 350–450 °C, the semi-coke's permeability increases dramatically [33]. The cracking and carbonization of residual organic matter in semi-coke becomes more intense at higher temperatures (≥ 430 °C). Furthermore, the cracked coke easily blocks the pores in the semi-coke, particularly the small pores [34].

As was already indicated, the majority of research concentrates on the combustion reaction of semi-coke at temperatures above 400 °C while ignoring the reaction properties of semi-coke below 400 °C. Thus, important research gaps on potentially the most appropriate temperature lower than 400 °C should be thoroughly

investigated. Meanwhile, the relationship between heat generation and demand in the underground reaction of the ATS process is unclear and the optimal temperature parameters are also unknown. This paper aims at filling these research gaps.

In this study, the calorific value, combustion kinetics, combustion properties, and product release characteristics of semi-cokes obtained from 225–520 °C were systematically studied. The combustion activation energy and combustion characteristic indices of various semi-cokes were determined; the heat relationship between heat generation and demand in the different reaction stages of the ATS process was clarified; an optimal temperature screening strategy and the optimal temperature parameters for Huadian OS ATS process were obtained. The purpose of this research is to provide a new perspective on the theoretical foundation of the ATS process and guidance and support for the actual ATS production process.

2. Methods and theory

2.1 Materials

The OS sample used in this study was acquired from Huadian, Jilin Province, China. The results of the proximate, ultimate, and Fischer assay analyses of raw OS used in this investigation are shown in Table 1. Each test was conducted three times, and the average value was then taken (Table S1). In order to obtain better homogeneity and reproducibility, the raw OS was crushed and screened into 0.4–1.7 mm-sized particles and fully dried in an oven at 80 °C for 10 hours for the subsequent experiments.

Table 1

The proximate, ultimate, and Fischer assay analysis results of the raw OS.

Proximate analysis (wt.%, ad)		Sd	Ultimate analysis (wt.%, d)		Sd
Moisture	4.26	0.09	C	22.20	0.15
Volatile matter	30.63	0.11	H	3.07	0.05
Ash	61.79	0.12	N	0.50	0.03
Fixed carbon	3.32	0.09	O	12.90	0.06
Calorific value (MJ/kg)	9.82	0.06			
Fischer assay analysis (wt.%, ad)					
Shale oil	14.91	0.07			
Water	5.57	0.04			
Semi-coke	72.16	0.12			
Gases + loss	7.36	0.08			

Note: ad: air dried, d: dried, Sd: Standard deviation.

2.2 Sample preparation

The experimental apparatus used in this study is shown in Fig. 2, and the experimental steps are as follows. First, 20 g of raw OS was placed on a wire mesh inside a quartz retort (inner diameter of 50 mm and height of 140 mm). The wire mesh was employed to ensure the nitrogen had a satisfactory purging effect for the output of oil and gas products. Next, the OS samples were heated from ambient temperature (20 ºC) to a specified temperature (225, 300, 330, 350, 370, 390, 410, 430, 450, and 520 ºC) with a heating rate of 10 ºC/min by an external heater in an N_2 atmosphere and then held for 2 hours to pyrolyze completely. The nitrogen flow rate was maintained at 50 ml/min by a flow control device which could effectively carry the oil and gas products out and avoid the temperature drop due to heat absorption.

During the experiment, the liquid products were condensed and collected in a condensation tank at −10 °C using an ethylene glycol aqueous solution. After pyrolysis, the liquid products and OS semi-cokes were successively collected and weighed when the apparatus had naturally cooled down to ambient temperature. The obtained oil-water mixture was weighed and subsequently separated by a toluene-water azeotrope for their yield calculation. The gas yield was calculated by the difference. Each experiment was repeated at least 3 times under the same conditions for stability and repeatability. Then the results with a difference of less than 5% among the three groups were chosen, and the average values obtained were the final yields.

For convenience, the raw OS was labeled as Sraw and the semi-cokes obtained at different pyrolysis temperatures were labeled as SN225, SN300, SN330, SN350, SN370, SN390, SN410, SN430, SN450, and SN520, respectively, where the “N” indicates the pyrolysis atmosphere was nitrogen and the latter number refers to the target pyrolysis temperature.

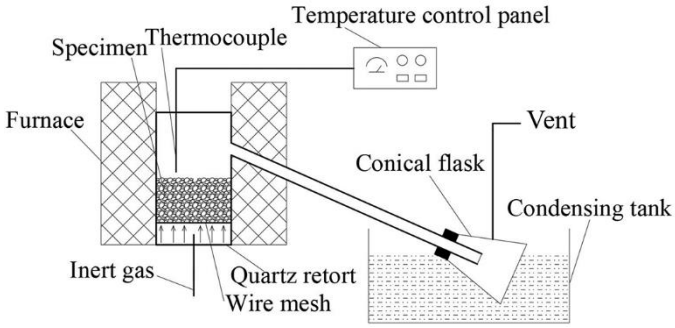

Fig. 2. Schematic diagram of the experimental apparatus.

2.3 Analytical methods

Thermogravimetric (TG) and differential scanning calorimetry (DSC) analyses of Sraw and semi-cokes were performed with an STA 449F3 thermal analyzer (Netzsch, Germany). Nitrogen was the protective gas with a flow rate of 20 ml/min, while N_2 or air was the carrier gas with a flow rate of 80 ml/min. A 20 mg (±0.5 mg) powder sample was used in each test to reduce the influence of temperature gradients and heat and mass transfer effects. The samples were heated from 30 to 900 °C at rates of 5, 10, and 20 °C/min. Duplicate experiments were performed to ensure reproducibility and the errors of mass loss and temperature were less than 0.5 wt% and 1 °C, respectively. The calorific values of Sraw and semi-cokes were determined under 3 MPa oxygen pressure by an XRY-1C automatic oxygen bomb calorimeter (Changji, China). Multiple calorific value measurements were performed in order to reduce the inhomogeneity and increase the reliability. The average value of three groups with an error of less than 5% was calculated and reported.

3 Theory

3.1 Kinetic triplets and equations

Kinetic analysis was performed to examine the kinetic parameters of Sraw and semi-cokes further. The fundamental rate equation can be described by Eq. (1) based on the Arrhenius equation as follows [35]:

$$\mathrm{d}\alpha/\mathrm{d}t = A\exp\left(-E_\alpha / RT\right) f\left(\alpha\right) \tag{1}$$

where, α is the degree of reaction; t is the time (min); A is the pre-exponential factor

(s^{-1}); E_α is the apparent activation energy (kJ/mol); R is the universal gas constant (R = 8.314 $J \cdot mol^{-1} \cdot K^{-1}$); T is the reaction temperature (K); $f(\alpha)$ is a reaction model function that describes the dependence of the reaction rate on the reaction extent.

The degree of reaction α can be represented as:

$$\alpha = (m_0 - m_t)/(m_0 - m_\infty) \quad (2)$$

where, m_0 is the initial mass of the sample, m_t is the sample mass at reaction time t, and m_∞ is the final mass of the sample.

The parameter β is introduced in the non-isothermal thermogravimetric method, and it is defined as:

$$\beta = dT/dt \quad (3)$$

The parameters of the kinetic triplet, E, A, and $f(a)$, are determined by the following three approaches during the kinetic analysis of solid-state reactions.

The Flynn-Wall-Ozawa (FWO) method employs Doyle's approximation for temperature integration [36]. Assuming the natural logarithm, the rearrangement obtains Eq. (4):

$$\ln \beta = \ln \frac{AE}{Rg(\alpha)} - 5.331 - 1.052 \frac{E}{RT} \quad (4)$$

In addition, the Friedman method is a differential equal conversion method with the following equation [35,37]:

$$\ln\left(\beta \frac{d\alpha}{dT}\right) = \ln Af(\alpha) - \frac{E}{RT} \quad (5)$$

On the other hand, the Kissinger-Akahira-Sunose (KAS) method uses the

following expression [35,37]:

$$\ln\frac{\beta}{T^2}=\ln\frac{AR}{Eg(\alpha)}-\frac{E}{RT} \tag{6}$$

where, $g(\alpha)$ is a reaction model similar to $f(\alpha)$, and E, β, T, R, and A have the same meaning as above. Under the same conversion at different temperature heating rates, the regression lines of $\ln\beta$ vs. $1/T$ for the FWO method, $\ln[\beta(\mathrm{d}\alpha/\mathrm{d}t)]$ vs. $1/T$ for the Friedman method, and $\ln(\beta/T^2)$ vs. $1/T$ produce the estimates of E from the slope for each conversion degree, which shows in Figs. 3b, 3c and 3d. Thus, the corresponding kinetic parameters were obtained from the TG data.

In general, the TG curves of Sraw and various semi-cokes in the air can be divided into three parts [20,37]. The second part of the TG curve mostly represents the decomposition and combustion of kerogen and remaining by-products, and the DTG curve can be used to calculate the reaction region. Fig. 3a depicts the TG and DTG results of Sraw at 5, 10, and 20 °C/min heating rates, as well as the reaction region of the second part [36]. Moreover, the TG and DTG results of various semi-cokes at heating rates of 5, 10, and 20 °C/min and the reaction region of the second part are presented in Fig. S1.

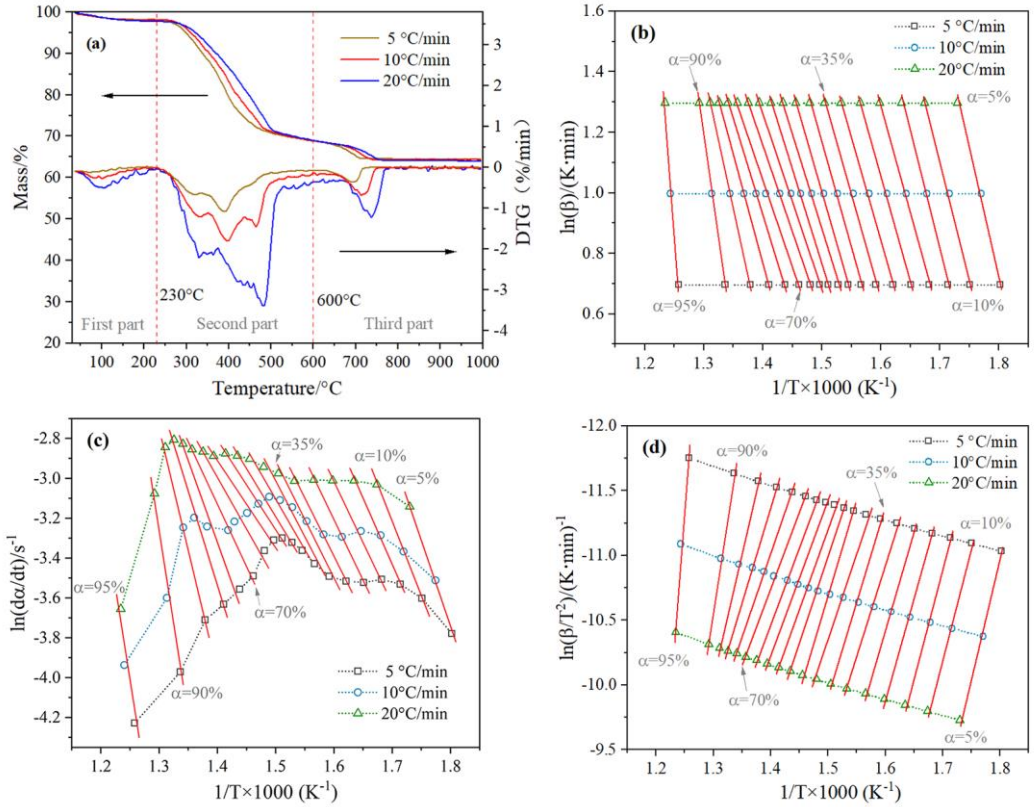

Fig. 3. (a) The TG and DTG results and the second-part reaction region of Sraw at heating rates of 5, 10, and 20 °C/min and the calculation curve of combustion activation energy by (b) FWO, (c) Friedman, and (d) KAS methods.

3.2 Combustion properties of semi-cokes

3.2.1 Combustion property parameters

According to the TG-DTG extrapolation method, the combustion property parameters of Sraw and various semi-cokes can be determined by drawing the TG-DTG curve in the following steps [27,38]. Firstly, through the point with the highest weight loss rate on the DTG curve, draw a vertical line to intersect the TG curve at point H as shown in Fig. 4. Secondly, make the tangent of the TG curve pass through point H and intersect with the baseline extension line at the initial missing point I in the second-part of the TG curve. The corresponding temperature at this intersection is

recorded as T_i, that is, the ignition temperature of the sample. Finally, the weight loss rate decreases steadily at point E, near the end of the second part of the TG curve. The tangent line passing through point H and the extension line at point E intersect at point T_e, that is, the burnout temperature of the sample. Similarly, the combustion characteristic parameters of various semi-cokes are also calibrated by the extrapolation method.

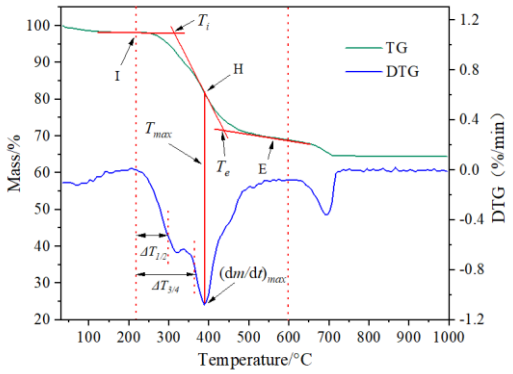

Fig. 4. Schematic diagram of extrapolation method to calibrate the combustion property parameters of Sraw (5 °C/min).

3.2.2 Combustion property indices

Based on the measurements of the TG-DTG curve of Sraw and various semi-cokes, the combustion index C, the combustion stability index R_w, and the comprehensive combustion index S are used to compare the combustion properties of Sraw and various semi-cokes.

The combustion index C reflects the reaction in the early stage of combustion and is defined as [39]:

$$C = \frac{(\mathrm{d}m / \mathrm{d}t)_{\max}}{T_i^2} \tag{7}$$

where, T_i is the ignition point of Sraw and various semi-cokes, °C; $(dm/dt)_{max}$ is the maximum weight loss rate of Sraw and various semi-cokes, %/min. The combustibility increases with the value of C, indicating that the sample is relatively more easily ignited, or has a relatively higher maximum weight loss rate.

Rw represents the stability of the combustion process, which is delineated as [27,40,41]:

$$R_w = \frac{655}{T_i} \times \frac{763}{T_{\max}} \times \frac{\left(\mathrm{d}m/\mathrm{d}t\right)_{\max}}{0.00582} \tag{8}$$

where, 655 is the ignition point of pure carbon, °C; 763 is the temperature corresponding to the maximum weight loss rate (0.00582) of pure carbon, °C; T_i is the ignition point, and T_{max} is the corresponding temperature of the maximum weight loss rate of Sraw and various semi-cokes, °C. The combustion stability of samples is increasing with the value of R_w, suggesting that, relatively, the samples have lower ignition points and T_{max}, as well as greater maximum weight loss rates.

The index of S can estimate the ignition, combustion, and burnout properties, and the calculation is as follows [27,41]:

$$S = \frac{\left(\mathrm{d}m/\mathrm{d}t\right)_{\max}\left(\mathrm{d}m/\mathrm{d}t\right)_{mean}}{T^2{}_i T_{\mathrm{e}}} \tag{9}$$

$$\frac{\mathrm{d}m}{\mathrm{d}t} = \frac{m_2 - m_1}{t_2 - t_1} \tag{10}$$

where, $(dm/dt)_{max}$ is the maximum weight loss rate and $(dm/dt)_{mean}$ is the average weight loss rate in the second stage of Sraw and various semi-cokes, %/min; T_e is the

burnout temperature, °C. The higher the values of *S*, the preferable the combustion performance of the sample is, showing relatively lower temperature parameters and higher weight loss rates.

3.3 Release index of combustion products

The products release index *r* is commonly used to define the difference between the release characteristics of combustion products and the reaction rate of solid fuels. Hence, *r* is utilized to analyze the combustion of Sraw and various semi-cokes in diverse places under non-isothermal conditions. The release characteristics of Sraw and various semi-cokes' combustion products with reaction rates of 50% and 75% in the second part are computed as follows [27,38,40]:

$$r_{1/2} = \frac{(\mathrm{d}m/\mathrm{d}t)_{\max}}{T_{\max} T_i \cdot \Delta T_{1/2}} \tag{11}$$

$$\Delta T_{1/2} \rightarrow \frac{\mathrm{d}m/\mathrm{d}t}{(\mathrm{d}m/\mathrm{d}t)_{\max}} = \frac{1}{2} \tag{12}$$

$$r_{3/4} = \frac{(\mathrm{d}m/\mathrm{d}t)_{\max}}{T_{\max} T_i \cdot \Delta T_{3/4}} \tag{13}$$

$$\Delta T_{3/4} \rightarrow \frac{\mathrm{d}m/\mathrm{d}t}{(\mathrm{d}m/\mathrm{d}t)_{\max}} = \frac{3}{4} \tag{14}$$

where, T_i, $(dm/dt)_{max}$, and T_{max} have the same meaning as above; $\Delta T_{1/2}$ is response to the half-peak temperature width of $(dm/dt)/(dm/dt)_{max}=1/2$, and $\Delta T_{3/4}$ is response to the three-fourths temperature width of $(dm/dt)/(dm/dt)_{max}=3/4$ (as shown in Fig. 4). They both indicate the release concentration of Sraw or semi-coke combustion products. The greater *r* indicates relatively lower temperature parameters, shorter

combustion time, and higher maximum weight loss rate, showing better combustion properties of Sraw or semi-cokes.

4. Results and discussion

4.1 Pyrolysis properties of oil shale

4.1.1. Yields of pyrolysis products

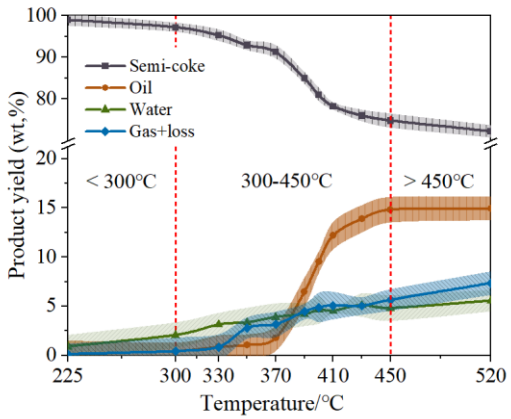

Fig. 5. Yields of oil shale pyrolysis products at different temperatures in nitrogen atmosphere.

In general, OS can be converted to oil, gas, water, and semi-coke through pyrolysis, and the yields will change as the temperature rises [18,22]. The decomposition process of kerogen in OS follows the pathway of kerogen > bitumen> oil + gas + semi-coke [42,43,44]. As seen in Fig. 5, OS produces a little water and nearly no oil and gas products at low temperatures (30–300 °C). The interlayer and crystallization water within the inorganic minerals and the small quantity of free bitumen in OS can be released at this temperature range, while the kerogen matter only has a certain swell or soften without further cracking [2,35]. When heated to 300–450 °C, the kerogen will continually crack into bitumen, and then into volatile oil and gas. It is worth noting that the yield of gas is significantly improved at 330–

350 °C, while the output of oil begins to accelerate after 370 °C. Finally, the yield of oil essentially stabilizes as the temperature rises (450–520 °C), suggesting that kerogen has been fully pyrolyzed [20,43].

4.1.2. Calorific value of semi-coke

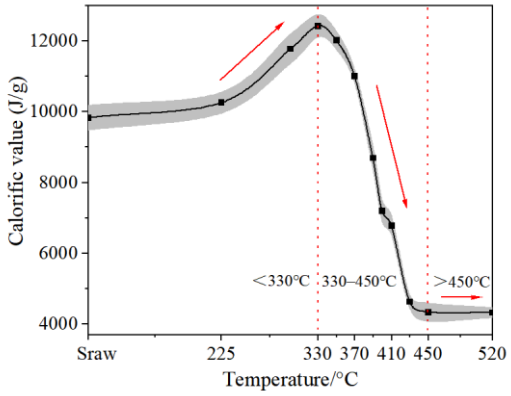

Fig. 6. Calorific values of Sraw and various semi-cokes pyrolyzed at different temperatures in nitrogen.

Through heat treatment at different temperatures, the calorific value of OS will change significantly in stages, which is related to the chemical composition change of semi-coke [18,45]. Fig. 6 shows the calorific value analysis results of the semi-cokes obtained at different pyrolysis temperatures. It is quite remarkable that, the calorific value of semi-coke gradually increases with heat treatment temperature, reaches a maximum at about 330 °C, then sharply decreases and remains at a low value above 450 °C. At first, the evaporation of water in OS slightly increased the calorific value caused by heating it to ~225 °C. After that, with the rise of heating temperature, the kerogen gradually softened and some fragments weakly bonded in the kerogen skeleton began to break and release, resulting in the formation of some primary macromolecular products [43,46,47]. These primary macromolecular pyrolyzes, that

is, the bitumen, had complex structures and high boiling points, suggesting that they would rarely volatilize from the OS matrix [44]. Furthermore, the bitumen had not yet begun to convert into volatile oil and gas at 300–330 °C. Therefore, the absorbed heat was stored in the organic matter inside of OS through the heat treatment, which indicates that heat treatment of ~330 °C can significantly improve the calorific value of OS.

Next, the calorific value of semi-coke from SN330 to SN450 decreases dramatically due to the further cracking of kerogen and bitumen and the massive release of the oil and gas products at a higher pyrolysis temperature. Thus, the heat stored in the OS was released in huge amounts in the form of oil and gas products. Finally, the calorific value of semi-coke almost reaches the lowest value and appears to be consistent after pyrolysis above 450 °C, indicating that the kerogen pyrolysis and hydrocarbon expulsion are essentially complete after the 2-hour pyrolysis. The non-volatile organic matter condensate produced by kerogen pyrolysis remains in the OS matrix, which is the main source of the calorific value of SN520 [20,21].

4.2 Evaluation of semi-coke combustion performance

4.2.1. Combustion property parameters analysis

Table 2 shows the reaction region of the second part of Sraw and various semi-cokes derived from DTG curves, as well as the relevant combustion property parameters.

Table 2

Combustion property parameters of Sraw and various semi-cokes obtained from TG results with a heating rate of 5 °C/min.

Sample	Reaction region of the second part/°C	T_i/ °C	T_e/ °C	ΔT [a]/ °C	T_{max}/ °C	$(dm/dt)_{max}$ %/min
Sraw [b]	230–600	314	436	122	388	1.078
SN225	229–609	374	480	106	461	1.302
SN300	232–600	317	444	127	381	1.092
SN330	238–600	346	484	138	461	0.907
SN350	231–600	324	459	135	394	1.113
SN370	240–600	325	459	134	401	1.067
SN390	229–600	330	450	120	401	0.943
SN410	266–600	343	454	111	391	0.768
SN430	270–600	348	443	95	391	0.753
SN450	263–610	358	451	93	396	0.656
SN520	303–615	382	470	88	423	0.628

[a] $\Delta T = T_e - T_i$; [b] dry basis

The ignition temperature (T_i) of the semi-coke is mainly related to the composition of the residual organic matter and the pore structure within it. Compared to Sraw, which was only dried at 80 °C, the ignition temperature of SN225 is significantly higher. This is due to the fact that as the water evaporated, the free bitumen originally present in the OS was also released. The loss of this flammable material will reduce the ignition characteristics of the semi-coke and greatly increase its ignition temperature [36]. Then more of the original bitumen was released as the temperature rose to 300 °C. However, the ignition temperature is drastically reduced as new bitumen was generated inside the semi-coke. Afterwards, a large amount of bitumen was produced at 330 °C, causing the volume of organic matter to expand and fill the pores [31–34]. Meanwhile, during ignition, the resulting bitumen tended to coke and block the pore exits [34,48]. Both of them result in a significant increase in

the ignition temperature of SN330. Following that, the pores reopened as higher heat treatment temperatures released more hydrocarbons from the OS. Finally, the condensation degree of the residual organic matter increased, resulting in a gradual increase in the ignition temperature. Similarly, the burnout temperature, T_e, exhibits basically the same variation as T_i.

In addition, the combustion temperature range (ΔT) of SN225 becomes significantly smaller due to the higher ignition temperature and water loss. Although SN330 has a higher ignition temperature as well, it has the largest ΔT due to severe pore blockage. After that, as the temperature exceeds 330 °C, ΔT becomes smaller and smaller due to the release of more and more organic matter during pyrolysis. Correspondingly, the largest $(dm/dt)_{max}$ occurs in the smaller ΔT of SN225 and a smaller $(dm/dt)_{max}$ occurs in the largest ΔT of SN330. At last, as the volatile content continues to decrease, the $(dm/dt)_{max}$ shows a tendency to become smaller and smaller.

4.2.2. Combustion activation energy analysis

Fig. 7 displays the combustion activation energies of various semi-cokes calculated using the Friedman, FWO, and KAS methods. The results indicate that the variations of activation energy obtained by these three methods are basically the same. The activation energy results obtained by FWO method are taken as an example for the further analysis.

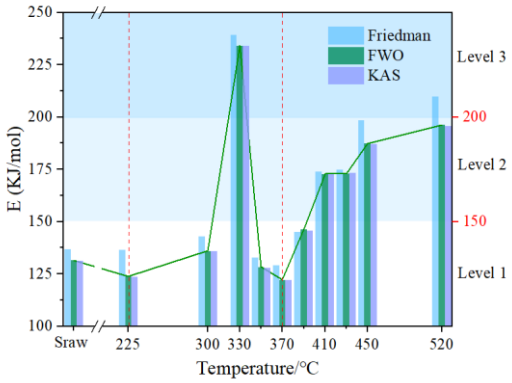

Fig. 7. Variation of combustion activation energy (based on TG results at a heating rate of 5 °C/min) obtained by the Friedman, FWO, and KAS methods for the Sraw and various semi-cokes.

As shown in Fig. 7, significant differences in the combustion activation energy of the semi-coke occurred with changes in heat treatment temperature. First, the activation energy decreases slightly from Sraw to SN225. The precipitation of interlayer water from Sraw to SN225 causes the appearance and enlargement of many microscopic pores in the inorganic minerals within the OS [31]. This increases the contact area of oxygen with the kerogen dispersed within the small pores, raising the possibility of a combustion reaction. Although the releasing of partial free bitumen increases the ignition point of SN225, the results show that the loss of water and high reaction temperature have a greater impact, leading to a faster and more intense combustion reaction, which can be shown by the smaller ΔT and the largest $(\mathrm{d}m/\mathrm{d}t)_{\max}$ of SN225 (Table 2).

Next, the activation energy shows a remarkable trend of first increasing and then dropping from SN300 to SN370. As the temperature rose above 300 °C, more free bitumen wrapped in organic matter was released, while the primary bitumen products

were generated. This primary product is a complex organic substance that will fill the internal pores of OS, resulting in a reduction in pore volume [31–34]. Moreover, bitumen is prone to coking reactions that produce considerable volumes of coke at the pore exits and plug the pore spaces upon ignition [34,44]. Therefore, the pore blockage due to the volume expansion of the generated bitumen and the coking during ignition results in an increase in the combustion activation energy of SN300. This blocking effect is most severe at SN330, which results in the maximum activation energy for combustion.

Finally, the activation energy increases with temperature from SN370 to SN520. As the kerogen's pyrolysis progresses to the over-matured stage, the organic matter is gradually condensed in the aromatic skeleton of the kerogen to form residual carbon, heavy components, and other less combustible components [20,21,43,44]. Thus, the combustion activation energy of semi-coke shows a steady upward trend. Although the porosity continues to rise due to the huge escape of oil and gas products at high temperatures, the change in chemical components clearly takes precedence.

The difficulty of combustion reactions of Sraw and various semi-cokes is divided into three levels based on the results of combustion activation energy (Fig. 7). Level 1 (<150 KJ/mol) has the easiest combustion reaction, followed by level 2 (150–200 KJ/mol), and level 3 (>200 KJ/mol) has the most difficult combustion reaction.

4.2.3. Combustion property indices analysis

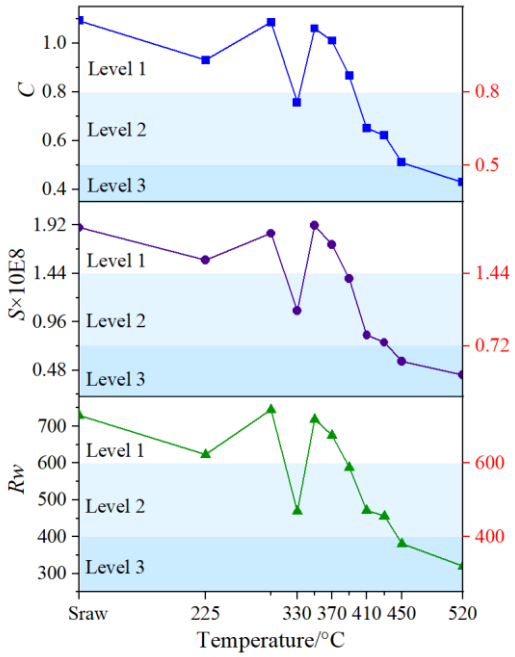

Fig. 8. The combustion index *C*, comprehensive combustion index *S*, and combustion stability index R_w of Sraw and various semi-cokes.

Fig. 8 displays the calculated results of the combustion index *C*, the combustion stability index R_w, and the comprehensive combustion index *S* of the Sraw and various semi-cokes. In general, the sample's combustion property improves as these indices rise. As shown in Fig. 8, these three indices indicate the same tendency of fluctuation. They all fluctuate for several times before 350 ºC and then gradually decrease as the heat treatment temperature rises.

The small molecular free bitumen in OS plays a significant role in the combustion process [36]. At first, the release of this free bitumen makes the ignition of SN225 more difficult and reduces its combustion performance. Later, kerogen is converted to a portion of the primary product bitumen at 300 °C, resulting in a slight improvement in the combustion performance of SN300 [35]. However, due to severe

pore blockage caused by the generation of a considerable amount of bitumen and ignition coking, the combustion performance of SN330 is seriously reduced. Afterwards, the interior pore space of semi-coke is enlarged once more as a result of the further cracking and releasing of products. Moreover, the small hydrocarbons cracked from bitumen increase the combustion performance of SN350. Finally, with the release of the volatile matter via pyrolysis, the organic content in the semi-coke drops constantly from SN350 to SN520. Due to the increase in the proportion of uninflammable organic condensation products, the combustion process of the semi-coke has changed from homogeneous to non-homogeneous combustion, resulting in the combustion performance continuing to deteriorate [25,26].

Similarly, the combustion performance of semi-coke is split into three levels depending on the values of these indexes as shown. Level 1 indicates excellent combustion performance, level 2 denotes medium, and level 3 suggests poor combustion performance.

4.2.4. Release characteristics analysis of combustion products

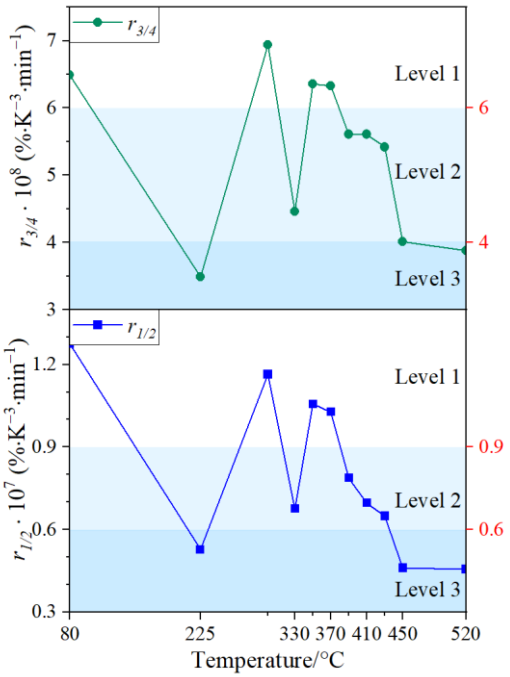

Fig. 9. The product release indices $r_{1/2}$ and $r_{3/4}$ of Sraw and various semi-cokes.

The combustion product release indices $r_{1/2}$ and $r_{3/4}$ of Sraw and various semi-cokes are depicted in Fig. 9. The results show the variation of $r_{1/2}$ and $r_{3/4}$ is remarkably comparable to the results of combustion property indices. First, the loss of free bitumen from Sraw to SN225 results in a considerable reduction in $r_{1/2}$ and $r_{3/4}$. Then, caused by the formation of bitumen and small-molecule products, the $r_{1/2}$ and $r_{3/4}$ increase again from SN225 to SN300. Similarly, the release characteristic of SN330 deteriorates due to substantial pore blockage by the significant amount of generated bitumen and coking during the ignition process. Later, because of the secondary conversion of bitumen and the escape of products, the pore space is reopened, leading to the increases of the $r_{1/2}$ and $r_{3/4}$ once more (SN350) [20,31,35]. Finally, as the volatile content diminishes and uninflammable by-products are formed,

the $r_{1/2}$ and $r_{3/4}$ gradually decrease from SN350 to SN520. Similarly, the product release indices were divided into three levels, as shown in Fig. 9.

4.3. Optimization of temperature parameters for ATS process

4.3.1. Endothermic characteristics of oil shale pyrolysis

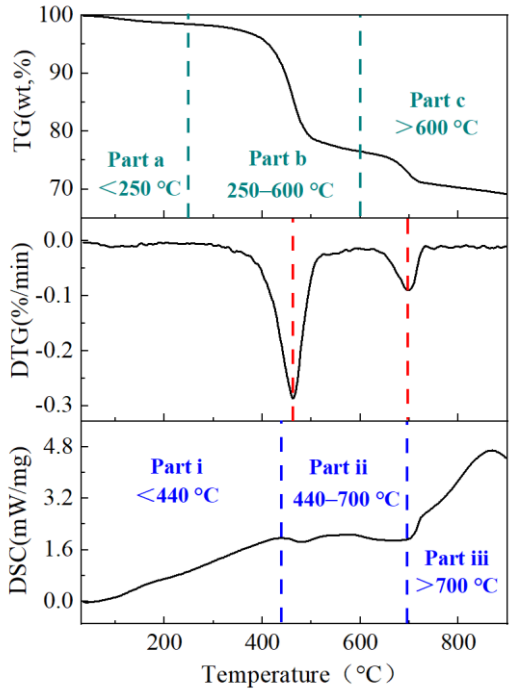

Fig. 10. TG/DTG/DSC curves of Sraw pyrolysis in nitrogen at a heating rate of 10 °C/min.

The TG/DTG/DSC curves of OS pyrolysis in a nitrogen atmosphere are shown in Fig. 10. The results indicate that the TG curve has three separate parts, each representing a different composition transition [20,21]. Interlayer water evaporates in part a, kerogen is pyrolyzed in part b, and mineral components such as carbonate are decomposed in part c [35]. Relatively, there are two distinct peaks on the DTG curve. The first strong peak appears at 460 °C, corresponding to the maximum pyrolysis rate of kerogen in part b. The second strong peak comes at 700 °C, which corresponds to the maximal decomposition rate of carbonate and clay minerals in part c [35].

Similarly, the DSC curve demonstrates that the OS absorbs heat during the pyrolysis process and shows three parts. First, the part i of the DSC curve (< 440 °C) has a similar linear increasing feature. The heat absorption at this part is primarily used for the evaporation of interlayer water, the increase in internal energy of OS, and the cracking of partial kerogen. After that, the DSC curve shows a smooth characteristic at part ii (440–700 °C), indicating that the heat absorption has stabilized. At this stage, the pyrolysis of kerogen almost reaches its maximum, a large amount of absorbed heat is carried out by oil and gas products, and some carbonate and clay minerals begin to decompose [18,21]. Finally, the DSC curve shows a rapid increase at part iii (> 700 °C), which is attributed to the large amount of heat absorption by the decomposition of carbonate and clay minerals [20,21].

4.3.2. Heat balance temperature in ATS process

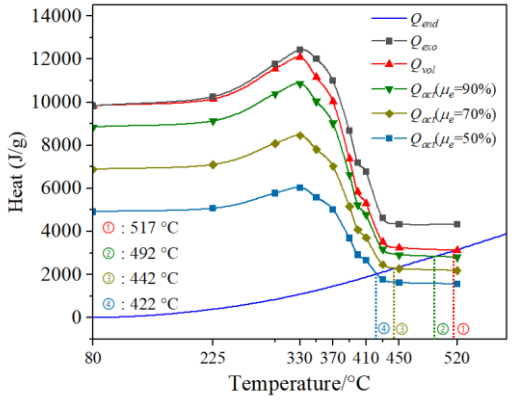

Fig. 11. Variation of endothermic heat for OS pyrolysis and heat release from semi-coke combustion with temperature.

During the ATS process, the semi-coke in the combustion zone (CZ in Fig. 1) is continually ignited to supply heat for the OS in the retorting zone (RZ in Fig. 1), so the OS in RZ is continuously pyrolyzed to yield hydrocarbons and new semi-cokes.

When the above reactions are repeated, a continuous chain reaction of ATS process is formed. As displayed in Fig. 1, except for the preheating stage in the first step, there is no external energy input in the subsequent initiation and reaction stages. Therefore, it is required to ensure that the heat generated by the semi-coke combustion in CZ is adequate to heat the OS in RZ to the specified temperature, hence maintaining the continuous reaction and a considerable product yield. To better clarify the energy relationship in the ATS process, three energy concepts are defined independently as follows.

$$Q_{end}(OS)=\begin{cases} Q_{exo}(SC), & T=T_{mas} \\ Q_{vol}(SC)=\mu_y Q_{exo}(SC), & T=T_{vol} \\ Q_{act}(SC)=\mu_e\mu_y Q_{exo}(SC), & T=T_{act} \end{cases} \tag{15}$$

Where, $Q_{end}(OS)$ refers to the endothermic quantity required when a unit mass of OS is heated to the specified temperature T, J/g, as determined by integrating the DSC curve of OS in nitrogen; $Q_{exo}(SC)$ is the exothermic quantity that can be released by the complete combustion of a unit mass of semi-coke obtained after a full pyrolysis at T, J/g, as measured by an oxygen bomb calorimeter (Fig. 6); $Q_{vol}(SC)$ means the exothermic quantity that is released by the complete combustion of the corresponding mass of semi-coke obtained from the pyrolysis of a unit mass of OS at T, J/g; μ_y is the yield coefficient, which is equal to the yield of semi-coke at T (Fig. 5); $Q_{act}(SC)$ refers to the heat actually used to heat the OS in the front retorting zone derived from the combustion heat of the corresponding mass of semi-coke, J/g; μ_e is the energy efficiency coefficient, which measures the effective utilization rate of semi-coke

combustion heat; T_{mas} is the corresponding temperature when $Q_{exo}(SC)$ and $Q_{end}(OS)$ are equal, °C; T_{vol} is the corresponding temperature when $Q_{vol}(SC)$ and $Q_{end}(OS)$ are equal, °C; T_{act} is the corresponding temperature when $Q_{act}(SC)$ and $Q_{end}(OS)$ are equal, °C.

According to Eq. (15), when the temperature reaches T_{mas}, the heat produced by the combustion of a unit mass semi-coke formed at T_{mas} just satisfies the need for a unit mass OS's temperature to rise from room temperature to T_{mas}. As shown in Fig. 11, the exothermic curve $Q_{exo}(SC)$ of semi-coke and the endothermic curve $Q_{end}(OS)$ of OS do not overlap before 520 °C, indicating that T_{mas} is greater than 520 °C. However, the mass and volume of OS will decrease when it is pyrolyzed to semi-coke. For example, after pyrolysis at 520 °C, the mass of the semi-coke generated from 1g of OS is 72.18 % × 1g = 0.7218 g, as presented in Fig. 5. This means that the mass of semi-coke per unit volume in the combustion zone after pyrolysis will be much lower than the original OS before pyrolysis, resulting in a lower heat value per unit volume. Therefore, the yield coefficient μ_y is employed to modify the $Q_{exo}(SC)$ curve, and then the heat production curve of a unit volume semi-coke during the in-situ conversion process, $Q_{vol}(SC)$, is obtained. Because of this, the volume equilibrium temperature of heat, T_{vol}, is found at the intersection of $Q_{vol}(SC)$ and $Q_{end}(OS)$, which is 517 °C in Fig. 11.

Furthermore, in addition to the factor of heat exchange efficiency, there are also some negative factors that affect the utilization of combustion heat in practice. First,

although the majority of the combustion heat is carried to the front OS retorting zone through the injected gas, some heat will be lost to the upper and lower caprocks of the working OS formation. Second, the temperature of the injected gas is significantly lower than that of the combustion zone. As a result, the injected gas will first absorb a large amount of heat when entering the combustion zone, which will inevitably affect the reaction in the combustion zone to a certain extent. Furthermore, the output exhaust gas will also carry a large amount of heat within it. Finally, the uneven distribution of the pores and fractures formed during the reservoir stimulation process in the formation might easily result in insufficient combustion of semi-coke in some areas, reducing the output of combustion heat.

As a result, the calorific value of semi-coke cannot be fully utilized due to the foregoing and other potentially adverse factors. Thus, a coefficient heat utilization efficiency, μ_e, is defined as the ratio of semi-coke combustion heat available for the OS pyrolysis in RZ. Among the heat of complete combustion of a unit volume of semi-coke in CZ, the heat available for OS pyrolysis in RZ is represented by the product of $Q_{exo}(SC)$, μ_y, and μ_e, known as $Q_{act}(SC)$. When $Q_{act}(SC)$ equals $Q_{end}(OS)$, the temperature value associated with it is defined as T_{act} in Eq. (15). That is, in an actual engineering situation, controlling the highest temperature in RZ to T_{act} just satisfies the energy balance for the autothermic chain reaction in the ATS process. T_{act} is 492 °C when μ_e is 90%, 442 °C at 70%, and 422 °C at 50%, as shown in Fig. 11.

4.3.3. Screening strategy for optimized temperature parameters

As can be seen above, different stages of the ATS process have different reaction characteristics and regulatory requirements, allowing for the formulation of a reasonable temperature parameter screening strategy. However, before discussing, a few basic assumptions must be made due to the complexity of the actual formation, as indicated below:

- The properties of OS in different areas of the formation, including oil content and density, are similar;
- The distribution of OS in the formation is similar to that shown in Fig. 1, which is equally distributed in the horizontal direction;
- The target OS formation has undergone reservoir stimulation before exploitation, and the influence of large fractures and groundwater in formation has been eliminated, which can ensure the normal operation of ATS process.

According to the proposed strategy below, the reaction properties of semi-coke, and the above assumptions, the optimal temperature parameters could be determined. Firstly, in the preheating stage of the ATS process, a large amount of external energy needs to be input into the target formation to heat the OS to a critical state that is easily initiated. Thus, selecting a preheating temperature of T_0 is critical for the ATS process to effectively transition from the preheating stage to the initiation stage. Secondly, a certain amount of oil and gas products will remain inside the OS

formation in the early initiation stage, which can be ignited together with the semi-coke after the injection of the oxygen-containing gas. The heat can thus be used for the pyrolysis of the OS in RZ, implying that the preheating temperature T_0 does not have to be lower than T_{act}. Moreover, the ignition point, combustion performance, activation energy, and product release characteristics of semi-coke should meet certain requirements in order to achieve the desired initiating effect. In summary, the following are the preferred requirements for preheating temperature T_0.

- T_0 must be higher than the ignition temperature of the semi-coke obtained via the pyrolysis of OS at T_0;
- Semi-coke obtained at T_0 has a low activation energy (level 1);
- Semi-coke obtained at T_0 has good combustion performance (level 1);
- Semi-coke obtained at T_0 has good product release characteristics (level 1);
- T_0 does not have to be lower than T_{act}.

According to the preceding analysis, the optimal T_0 of Huadian OS is determined at temperatures of 350–370 °C.

The key to the reaction stage in the implementation of the ATS process is to obtain a higher oil and gas yield on the premise of maintaining autothermic pyrolysis reaction underground. Therefore, it is very important to regulate the maximum temperature (T_1) in RZ during the reaction stage. In general, T_1 should preferably meet the following requirements.

- Semi-coke produced at T_1 has a low activation energy (level 1);

- Semi-coke produced at T_1 has good combustion performance (level 1);
- Semi-coke produced at T_1 has good product release characteristics (level 1);
- T_1 must be less than or equal to T_{act}.

The most preferred value of T_1 appears to be T_{act}, which is influenced by μ_e. As shown in Fig. 11, the ideal T_1 of Huadian OS is 492, 442, and 422 °C when μ_e is 90%, 70%, and 50%, respectively. It can be seen from Fig. 5 that the oil yield is 13.42% and the gas yield is 5.01% when OS is pyrolyzed at 422°C, accounting for 89.89% and 68.25% of the total oil and gas yield, respectively. This indicates that the ATS process can meet oil and gas production demand even when the effective utilization rate of combustion heat is low, which also demonstrates the theoretical feasibility of in-situ OS extraction by the ATS process.

To sum up, a temperature control strategy for the ATS process which is applicable to a wide variety of OS formations was put forward. First, before the actual project, relevant experiments and field tests should be completed to determine the value of μ_e and the corresponding T_0 and T_{act}. Then, at the preheating stage of the ATS process, external heat is injected into the target OS layer after the reservoir stimulation process to preheat a certain area of OS close to the heat injection well to T_0. After that, ambient temperature oxygen-containing gas can be injected to initiate the oxidation and heat release reaction of the preheated OS, further inducing the autothermic pyrolysis chain reaction underground. Finally, the maximum temperature in RZ can be basically regulated to the T_{act} by altering the composition, flow, pressure,

injection time, and other parameters of the oxygen-containing gas. As a result, the autothermic pyrolysis chain reaction can be pushed forward continuously underground to ensure the continuous and effective production of oil and gas.

However, the distribution of underground temperature fields in the actual process is complex and changeable, which differs considerably from the assumption. The factors like preheating time and formation conditions should be thoroughly considered during actual production. In addition, the change of formation stress and thermal stress in OS formation during construction is also very important for ATS process, and should be paid attention to at all times during actual construction [49,50,51,52]. In this research, the reaction process was simplified by simple hypothesis analysis, and some fundamental conclusions and analysis were obtained, aiming to provide a new perspective on the theoretical basis as well as guidance and support for the actual ATS production process.

5. Conclusions

To explore the oxidation reaction characteristics of different semi-cokes in the OS ATS process and optimize the appropriate temperature parameters, the calorific value, combustion performance, and product release characteristics of semi-cokes obtained at different pyrolysis temperatures were systematically investigated. The primary results can be summarized as below: (1) Kerogen would continuously crack into bitumen and then become volatile oil and gas when heated to 300–450 °C. At 330-350 °C, the production of shale gas is significantly increased, while the

production of shale oil starts to accelerate when the temperature is greater than 370 °C. (2) With the pyrolysis temperature, the semi-coke's calorific value goes through three different stages of increasing, decreasing, and flattening, peaking at around 330 °C. The absorbed heat is stored in the organic matter inside OS, resulting in a large conversion of kerogen to bitumen during pyrolysis at this temperature. (3) The significant reduction in the reaction performance of the semi-coke is obtained at about 330 °C due to the clogged pores caused by plenty of bitumen generated and the bitumen coking during the ignition. In the high temperature section (> 350 °C), the reaction performance decreases continuously due to the large reduction of the remaining volatile content and the generation of residual carbon and heavy components in the semi-coke. (4) The temperature corresponding to the balance between the combustion heat of semi-coke and the heat required for process operation during in-situ exploitation of Huadian OS is 517, 492, 442, and 422 °C, respectively, when the heat utilization rate is 100%, 90%, 70%, and 50%. (5) According to the optimal temperature screening strategy given in this study, the preferred preheating temperature range is 350–370 °C and the retorting temperature is T_{act} for Huadian OS. The results of this research provide a new perspective on the theoretical basis of the ATS process and have certain guiding significance for actual engineering.

Acknowledgements

This work was supported by the National Key R&D Program of China (No. 2019YFA0705502, 2019YFA0705501), the Young and Middle-aged Excellent Team

Project for Scientific and Technological Innovation of Jilin Province, China, the National Natural Science Foundation of China (42202345), and the National Natural Science Foundation of China (Grant No. 41972324, 52074212).

References

[1] Zhai YM, Zhu YM, Cui S, Tao YM, Kai XP, Yang TH. Study on the co-pyrolysis of oil shale and corn stalk: pyrolysis characteristics, kinetic and gaseous product analysis. Journal of Analytical and Applied Pyrolysis 2022; 163:105456.

[2] He L, Ma Y, Yue CT, Wu JX, Li SY. Kinetic modeling of Kukersite oil shale pyrolysis with thermal bitumen as an intermediate. Fuel 2020; 279:118371.

[3] Jarosław K, Alicja KN, Krzysztof G. The criticality of crude oil for energy security: a case of Poland. Energy 2021; 220:119707.

[4] Liu Z, Jiang X, Dai J, Wu M, Chen R. Overview of the domestic and foreign oil and gas industry development in 2020 and outlook for 2021. International Petroleum Economics 2021; 29(1):28–37.

[5] Amer MW, Alhesan JSA, Marshall M, Fei Y, Jackson WR, Chaffee AL. Energy efficient method of supercritical extraction of oil from oil shale. Energy Conversion and Management 2022; 252:115108.

[6] Kuang WQ, Lu MK, Yeboah I, Qian G, Duan XZ, Yang J, Chen D, Zhou XG. A comprehensive kinetics study on non-isothermal pyrolysis of kerogen from Green River oil shale. Chemical Engineering Journal 2019; 377:120275.

[7] He WT, Sun YH, Shan XL. Organic matter evolution in pyrolysis experiments of oil shale under high pressure: guidance for in situ conversion of oil shale in the Songliao Basin. Journal of Analytical and Applied Pyrolysis 2021; 155:105091.

[8] Kang SJ, Sun YH, Deng SH, Li SL, Su YZ, Guo W, Li JS. Extraction of Huadian oil shale in subcritical $FeCl_2$ solution. Fuel Processing Technology 2021; 211:106571.

[9] Zhu CF, Guo W, Sun YH, Li Q, Deng SH, Wang Y, Cui GD. Reaction mechanism and reservoir simulation study of the high-temperature nitrogen injection in-situ oil shale process: a case study in Songliao Basin, China. Fuel 2022; 316:123164.

[10] Kang ZQ, Zhao YS, Yang D. Review of oil shale in-situ conversion technology. Applied Energy 2020; 269:115121.

[11] Jaber TS, Apostolos K. A comprehensive review of microwave application on the oil shale: prospects for shale oil production. Fuel 2021; 305:121519.

[12] Kang Z, Xie H, Zhao Y, Zhao J. The feasibility of in-situ steam injection technology for oil shale underground retorting. Oil Shale 2020; 37(2):119.

[13] Martins MF, Salvador S, Thovert JF, Debenest G. Co-current combustion of oil shale-Part 1: characterization of the solid and gaseous products. Fuel 2010; 89:144–151.

[14] Guo HF, Peng SY, Lin JD, Chang J, Lei S, Fan TB, Liu YY. Retorting oil shale by a self-heating route. Energy Fuels 2013; 27:2445–51.

[15] Guo HF, Cheng QX, Wang D, Jin Z, Ding Y, Pei YS, Zhui H, Liu YY. Analyzing the contribution of semicokes to forming self-heating in the oil-shale self-heating retorting process. Energy & Fuels 2016; 30(7):5355–5362.

[16] Sun YH, Bai FT, Lü XS, Li Q, Liu YM, Guo MY, Guo W, Liu BC. A novel energy-efficient pyrolysis process: self-pyrolysis of oil shale triggered by topochemical heat in a horizontal fixed bed. Scientific Reports 2015; 5:8290.

[17] Sun YH, Bai FT, Liu BC, Liu YM, Guo MY, Guo W, Wang QW, Lü XS, Yang F,

Yang Y. Characterization of the oil shale products derived via topochemical reaction method. Fuel 2014; 115:338–346.

[18] Guo W, Yang QC, Sun YH, Xu ST, Kang SJ, Lai C, Guo MY. Characteristics of low temperature co-current oxidizing pyrolysis of Huadian oil shale. Journal of Analytical and Applied Pyrolysis 2020; 146:104759.

[19] Guo W, Yang QC, Zhang X, Xu ST, Deng SH, Li Q. Thermal behavior of oil shale pyrolysis under low-temperature co-current oxidizing conditions. ACS Omega 2021; 6(28):18074–18083.

[20] Xu ST, Sun YH, Lü XS, Yang QC, Li Q, Wang ZD, Guo MY. Effects of composition and pore evolution on thermophysical properties of Huadian oil shale in retorting and oxidizing pyrolysis. Fuel 2021; 305:121565.

[21] Guo HF, Pei YS, Wang KK. Identifying the reaction mechanism of oil-shale self-heating retorting by thermal analysis techniques. Fuel 2015; 160:255–264.

[22] Sun YH, Xu ST, Yang QC, Lai Cheng, Guo MY. Oxidizing pyrolysis of Huadian oil shale and its product distribution. J China Univ Pet (Edition of Natural Science) 2021; 45(2):149–156.

[23] Yang QC, Guo MY, Guo W. Effects of associated minerals on the co-current oxidizing pyrolysis of oil shale in a low-temperature stage. ACS Omega 2021; 6(37):23988–23997.

[24] Han XX, Jiang XM, Cui ZG, Liu JG, Yan JW. Effects of retorting factors on combustion properties of shale char. 3. distribution of residual organic matters. Journal of Hazardous Materials. 2010; 175:445–451.

[25] Jiang XM, Han XX, Cui ZG. Progress and recent utilization trends in combustion of Chinese oil shale. Progress in Energy and Combustion Science 2007;

33(6):552–579.

[26] Han XX, Jiang XM, Cui ZG. Study of the combustion mechanism of oil shale semicoke in a thermogravimetric analyzer. J Therm Anal Calorim 2008; 92:595–600.

[27] Zhao S, Sun YH, Lü XS, Li Q. Energy consumption and product release characteristics evaluation of oil shale non-isothermal pyrolysis based on TG-DSC. Journal of Petroleum Science and Engineering 2020; 187:106812.

[28] Bai FT, Zhao JM, Liu, YM. An investigation into the characteristics and kinetics of oil shale oxy-fuel combustion by thermogravimetric analysis. Oil shale 2019; 36(1):1–18.

[29] Han XX, Jiang XM, Cui ZG, Yan JW, Liu JG. Effects of retorting factors on combustion properties of shale char. J Therm Anal Calorim 2011; 104:771–779.

[30] Bai FT, Sun YH, Liu YM, Li Q, Guo MY. Thermal and kinetic characteristics of pyrolysis and combustion of three oil shales. Energy Conversion and Management 2015; 97:374–381.

[31] Bai FT, Sun YH, Liu YM, Guo MY. Evaluation of the porous structure of Huadian oil shale during pyrolysis using multiple approaches. Fuel 2017; 187:1–8.

[32] Liu ZJ, Yang D, Hu YQ, Zhang JW, Shao JX, Song S, Kang ZQ. Influence of in situ pyrolysis on the evolution of pore structure of oil shale. Energies 2018; 11(4):755.

[33] Yang LS, Yang D, Zhao J, Liu ZH, Kang ZQ. Changes of oil shale pore structure and permeability at different temperatures. Oil Shale 2016; 33(2):101.

[34] Han XX, Jiang XM, Yan JW, Liu JG. Effects of retorting factors on combustion properties of shale char. 2. pore structure. Energy & Fuels 2011; 25(1):97–102.

[35] Bai FT, Guo W, Lü XS. Kinetic study on the pyrolysis behavior of Huadian oil shale via non-isothermal thermogravimetric data. Fuel 2015; 146:111–118.

[36] Sun YH, Bai FT, Lü XS, Jia CX, Wang Q, Guo MY, Li Q, Guo W. Kinetic study of Huadian oil shale combustion using a multi-stage parallel reaction model. Energy 2015; 82:705–713.

[37] Bai FT, Sun YH, Liu YM. Thermogravimetric analysis of Huadian oil shale combustion at different oxygen concentrations. Energy & Fuels 2016; 30(6):4450–4456.

[38] Wang CA, Du YB, Che DF. Reactivities of coals and synthetic model coal under oxy-fuel conditions. Thermochimica Acta 2013; 553:8–15.

[39] Liao XJ, Zhang SH, Zhang X, Shao JA, Wang XH, Yang HP, Chen HP. Interaction and kinetics during the co-combustion process of coal slime, coal gangue and slack coal. Journal of China Coal Society 2021; 46(101):457–467.

[40] Wang Q, Jia CX, Jiang QQ, Wang Y, Wu DY. Combustion characteristics of Indonesian oil sands. Fuel Processing Technology 2012; 99:110–114.

[41] Zhang Q, Fang J, Meng ZW, Chen C, Qin ZH. Thermogravimetric analysis of soot combustion in the presence of ash and soluble organic fraction. RSC Advances 2020; 10(55):33436–33443.

[42] Hubbard A, Robinson W. A thermal decomposition study of Colorado oil shale. US Dept. of the Interior, Bureau of Mines 1950.

[43] Lai DG, Zhan JH, Tian Y, Gao SQ, Xu GW. Mechanism of kerogen pyrolysis in terms of chemical structure transformation. Fuel 2017; 199: 504–511.

[44] Zhan HL, Qin FK, Chen ST, Chen R, Meng ZH, Miao XY, Zhao K. Two-step

pyrolysis degradation mechanism of oil shale through comprehensive analysis of pyrolysis semi-cokes and pyrolytic gases. Energy 2022; 241:122871.

[45] Yang QC, Zhang X, Xu ST, Wang ZD, Guo W. Low-temperature co-current oxidizing pyrolysis of oil shale: study on the physicochemical properties, reactivity and exothermic characters of semi-coke as heat generation donor. Journal of Petroleum Science and Engineering 2022; 216:110726.

[46] You YL, Han XX, Wang XY, Jiang XM. Evolution of gas and shale oil during oil shale kerogen pyrolysis based on structural characteristics. Journal of Analytical and Applied Pyrolysis 2019; 138:203–210.

[47] You YL, Wang XY, Han XX, Jiang XM. Kerogen pyrolysis model based on its chemical structure for predicting product evolution. Fuel 2019; 246:149–159.

[48] Khansari Z, Kapadia P, Mahinpey N, Gates I. A new reaction model for low temperature oxidation of heavy oil: experiments and numerical modeling. Energy 2014; 64:419–428.

[49] Xu Y, Lun ZM, Wang HT, Zhou X, Zhao CP, Zhang GL, Zhang DF. Influences of controlled microwave field irradiation on occurrence space and state of shale oil: Implications for shale oil production. Journal of Petroleum Science and Engineering 2022; 219: 111067.

[50] Yang D, Wang GY, Kang ZQ, Zhao J, Lv YQ. Experimental investigation of anisotropic thermal deformation of oil shale under high temperature and triaxial stress based on mineral and micro-fracture characteristics. Nat Resour Res 2020; 29: 3987–4002.

[51] Wang JF, Liu YK, Yang C, Jiang WM, Li Y, Xiong YQ, Peng PA. Evolution of

mechanical properties of kerogen with thermal maturity. Marine and Petroleum Geology 2022; 145:105906.

[52] Wang ZL, Guo XY, Zheng GQ, Yu PR, Wang W, Jin Y, Chen G. Effects of parent well spacing on the poroelastic behaviors in the infill zone in shale oil reservoirs: a case study in Jimsar shale oil, China. Energy Science & Engineering 2022; 10(4): 1043–1054.